Folded Comb-line Array for Backscattering-based Bodycentric Communications in the 5G sub-6 GHz Band

Cecilia Occhiuzzi*, Jack D. Hughes†, Francesco R. Venturi*, John Batchelor†, Gaetano Marrocco*

Abstract—Growing interest in IoT and Healthcare pushes the exploration of innovative solutions for connecting our bodies to external systems. The need for devices interoperability combined with data rate considerations, and low power consumption make 5G backscattering-based communications a promising opportunity, especially in the low sub-6 GHz band. Starting from a monolithic array, this paper proposes a skin-mountable miniaturized antenna suitable for 3.6 GHz body-centric backscattering communications. The array is an improved version of the comb-line antenna, which simultaneously optimizes size and radiation features. The horizontal segments are folded such to place the radiating dipoles closer and increase the radiation efficiency of the structure by co-phasing a single component of the surface currents. Parametric analysis obtains optimal configurations in terms of gain and size. Compared to conventional layout, the miniaturized array has an efficiency 6 dB higher and an area 80% smaller while the improved structure provides a theoretical read distance of more than 4 m. Measurements on a volunteer corroborate the improved performance.

Index Terms—Wearable antenna array, backscattering communication, 5-G.

I. INTRODUCTION

Healthcare Internet of Things (H-IoT) is providing the backbone of the emerging Precision Medicine initiative by means of sensors connected to our bodies linked with everyday devices such as smartphones and smart watches [1]. In recent years, Radiofrequency Identification (RFID) technology, especially in the UHF band, has been enabling this technological framework [2]. However, the limited bandwidth and bit-rate at UHF, combined with the need for devoted readers to interact with the sensors stimulated the exploration of new backscattering-based monitoring platforms [3].

An attractive opportunity comes from the introduction of fifth generation (5G) wireless communications, where protocols allow for large bandwidth, low latency (1ms), and multigigabit-per-second (Gbps) data rates [4]. Adopting 5G into the H-IoT would hence encourage the development of innovative smart-healthcare devices [5], especially by taking advantage of the envisaged improvement in communication standards and interoperability between platforms [6]. Preliminary studies have demonstrated that the new 5G band at 3.6 GHz (n78, 3300-3800 MHz frequency band) grants performance improvements over UHF RFID for backscattered links, especially in cases involving wearable tags [7]. A single loop antenna directly adhering to the skin could be readable at up to 1 m [8]. Multiple elements arranged in an array configuration could offer robust coverage in a medium-sized room [7], but with the cost of increasing complexity with the need to host a beam forming network that could impact on size, fabrication and wearability. To simplify the layout, monolithic arrays such as the Krauss Grid [9] have recently been proposed for this application. In this layout, the radiating and transmission line elements are limited to a singular, easily fabricated layer and the array can be fed through only a single port. However, whilst the achieved radiation performances would be fully compliant with a medium-range body-centric communication link, the resulting size is large and therefore the monolithic array is only suitable for application on flat and large areas of the body, such as the abdomen, shoulders, and back.

A particular embodiment of a monolithic array is the comb-line [10]. Comb-line arrays are highly efficient radiators widely adopted for mm-wave automotive radar applications [11] and on-chip

integrated architectures [12]. They can be seen as a simplified version of the Krauss' grid [13], in which the transmission lines between the top of the vertical radiating elements are removed with benefits in terms of bandwidth and cross-polarization level. Tapered radiating microstrip elements are generally adopted [14], sometimes with sequential rotation for achieving circular polarization [15], while multiple sub-array configurations can be exploited for MIMO applications [16].

Starting from a comb-line antenna, this paper proposes for the first time a 3.6 GHz miniaturized monolithic array (layout in Fig. 1) for wearable body-centric communications. Authors presented early investigations on 3.6 GHz comb-lines antennas with improved radiation efficiency and reduced footprint in [17]. Numerical analysis on simplified body phantoms demonstrated the feasibility of the approach; however, a full investigation on the operating principal of the layout as well as the experimental characterization are still missing. The aim of this paper is hence to present a complete analysis on wearable comb-line monolithic arrays, from theoretical investigations and parametric studies up to measurements and validations on reference and real conditions.

The paper is organized as follows. In Section II the layout of the folded comb-line array is presented, together with a parametric analysis to identify the upper bound performances. Two optimal configurations are hence identified in terms of maximum gain and size reduction. The design of the miniaturized configuration is then described in Section III, together with prototype and experimental characterization. The performance of the layout in real conditions was evaluated by measurement campaign accounting for the conformability over curved surfaces and the placement on the body.

II. ANTENNA LAYOUT AND RATIONALE

Similarly to other monolithic arrays, the main limitation of the comb-line, especially at lower frequencies and for wearable applications, is the wide surface area caused by the presence of transmission line λ/2 segments which are required to enforce the proper pattern of current to the radiating elements. To the best of the authors' knowledge, no attempt has been made to miniaturize the structure while leaving unaffected the high radiation efficiency of the layout. Miniaturization of antennas is typically achieved by meandering the conductors [18] such to reduce the physical area of the structure while keeping the electrical area unmodified. However, meandering produces additional transmission-line segments in which currents with opposite phases are placed in close proximity. Such meandered portions do not contribute to radiation but do increase losses, especially in wearable applications due to the close proximity to the lossy human body. Hence, it is electromagnetically penalizing for the antenna efficiency to miniaturize the structure through meandering.

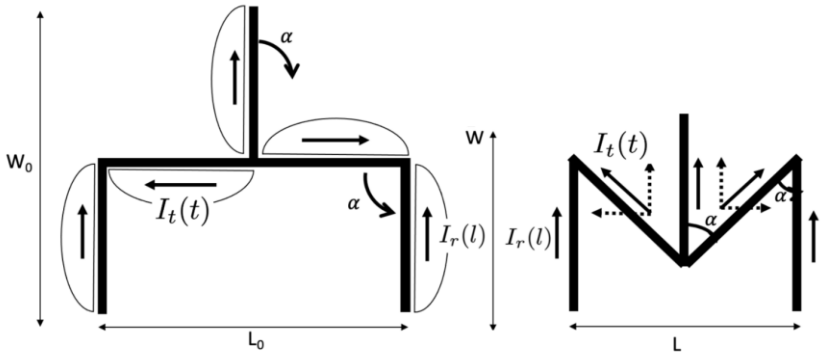

Fig. 1. Schematic representation of the folding effect on the pattern of currents and on the antenna size. Segments length $l \approx t \approx \lambda wg/2$ supports standing waves. The current amplitude has a peak every half-wavelength, with nulls on the nodes and on the extremities of each element.

Here, the proposed layout satisfactorily achieves miniaturization by a better exploitation of the transmission line segments in term of shape and current distribution, maintaining high radiation efficiency. By folding the horizontal elements with respect to the vertical elements (angle α in Fig. 1), a part of the transmission line current is also used for radiation. From this, two competing effects arise and impact on the radiation efficiency: the improvement of the antenna-mode of the structure and the electromagnetic coupling between close radiating elements. Optimal configurations can be hence defined.

A. Layout

The proposed layout comprises a microstrip array placed on a low loss dielectric slab (Fig. 2). Preferably, the dielectric substrate should be flexible and lightweight to enable placement on curved surfaces like the human body. Similarly to microstrip grid arrays [19], if properly designed, a typical microstrip comb-line is resonant: the currents $I_r(l)$ on the N vertical elements (with length $l \approx \lambda wg/2$) are in phase, whilst the currents $I_t(t)$ on the T = N − 1 guiding segments ($t \approx \lambda wg/2$) are piecewise in opposite phase. The array is fed in the middle of the central vertical element and placed on a dielectric slab backed by a ground plane. λwg is the guided wavelength [20] at the center frequency f_0 of operation, that is evaluated by considering the microstrip width w and the thickness h of the substrate that separates the comb-line from the ground plane [21]. A proper choice of the dielectric substrate in terms of complex permittivity $\bar{\epsilon}$ and thickness h leads microstrip lines to not have a bound field and consequently they can serve as radiating elements [22]. Radiation is sustained only by the vertical currents, since radiation arising from the horizontal guiding lines mutually cancel. Except for edge effects, there is no radiation in the rear direction.

Available space and conductors are not efficiently exploited since almost half of the conductors ((N − 1)/(2N − 1), i.e. the horizontal elements) do not contribute to the radiation but instead produce power losses. By acting on the folding angle α the mutual position between the elements changes and consequently so does the current distribution. Now the orientation of the previously horizontal track is more in-line with the radiating elements, a vertical current component $I_t^V(t) = I_t cos\alpha$ is generated by these oblique elements. Thus, depending on the folding angle α, additional current elements will sum in phase and the radiation will be enhanced and the efficiency improved. Furthermore, the folding of the horizontal strips produces miniaturization of both external sizes $L = L_0 sin\alpha$ and $W = W_0(1 - 1/2sin\alpha)$, where W_0 and L_0 are the width and length of the unfolded structure (α = 90◦), respectively. A better exploitation of conductors and available area is achieved.

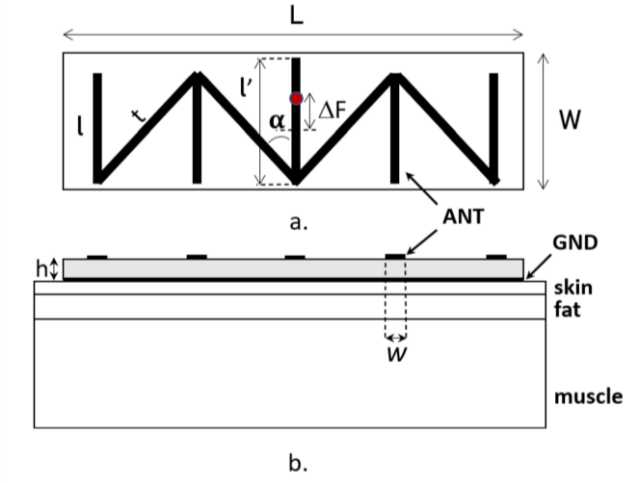

Fig. 2. Schematic representation of the folded comb-line antenna. Feed is shown as a red dot located at ΔF with respect to the midpoint of the central element a) Top view; b) Side view with the three-layer numerical body phantom adopted in FDTD simulations (CST Microwave Studio).

The proposed folded comb-line (Fig. 2 a) offers two degrees of freedom for optimizing size and radiation performances and two additional independent parameters for tuning the input impedance. The former are the number N of radiating elements and the folding angle α, whilst input impedance can be modified by acting on the length of the central segment l' and on the position ΔF of the feeding point with respect to the middle of the central element. The folded array is hereafter parametrically investigated. Analysis has been carried out through FDTD method (CST Microwave Studio). Simulations include a 150×150×th mm^3 3-layers planar body phantom [7] (Skin th = 1mm, εr = 36.92, tan δ = 2.08 - Fat th = 3mm, εr = 5.16, tan δ = 0.16 - Muscle th = 31mm, εr = 51.32, tan δ = 2.65 shown in Fig. 2 b).

B. Radiation performances

Starting from the 3-elements unfolded layout placed on a flexible dielectric slab with permittivity εr = 3 and tan δ = 2·10−3 (EccostockÂ® FlexK, by Laird), the number of vertical elements N and the folding angle α were progressively modified. Maximum gain G, radiation efficiency η and physical area AP = W × L are shown in Fig. 3.

As the number of elements in the array increases, so does the gain (Fig. 3 a). A maximum exists, regardless of the number of elements for α = 45◦. However, since efficiencies remain almost constant (shown by overlapping curves in Fig.3 b, in the α = 30◦ − 60◦ range), this effect is attributed to an increase in directivity caused by the enlargement of the antenna physical area with N, as visible in Fig. 3 c.

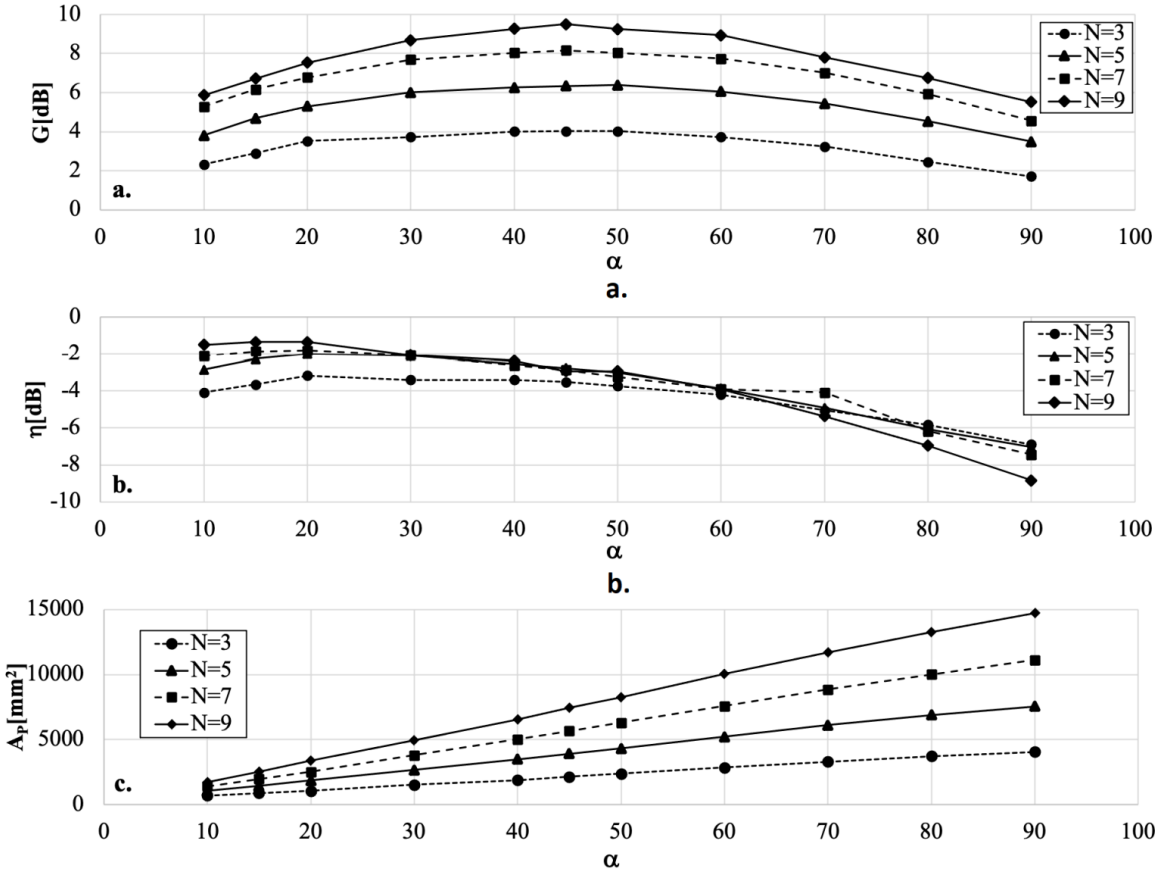

Fig. 3. Gain (a), radiation efficiency (b) and physical area (c) of the folded comb-line by varying the folding angle α and the number of elements N. Here {t = l = 28.55mm, w = 1mm, h = 1mm}.

The folding angle affects the radiation performance. Highly folded layouts compensate for the detrimental effect of the coupling with the benefits produced by the additional vertical current elements. Efficiency overall increases. An optimum $\eta \sim -2$ dB exists for $\alpha = [15^\circ - 40^\circ]$, corresponding to a spacing $s = t \cdot sin(\alpha)$ between vertical elements ranging between 7.38 mm and 18.3 mm. Further enlargements of the angle α reduces the vertical current components and increases the distance between the radiating elements, hence resulting in a reduction of the overall radiation efficiency and in an increase of overall size.

The beneficial effects of the folding on the radiation performance are visible in Fig.4 where the unfolded conventional layout ($\alpha = 90^\circ$) is compared with a highly folded layout ($\alpha = 15^\circ$). Regardless the number of elements, the gain and efficiency of the folded array are higher than the unfolded version. Furthermore, the folded layout better exploits the radiating elements since its efficiency increases at 0.73N. On the contrary, the unfolded layout suffers with the increase in radiating dipoles, with a decreasing trend in efficiency (scaling factor of $\eta_{90} \propto -0.6$N).

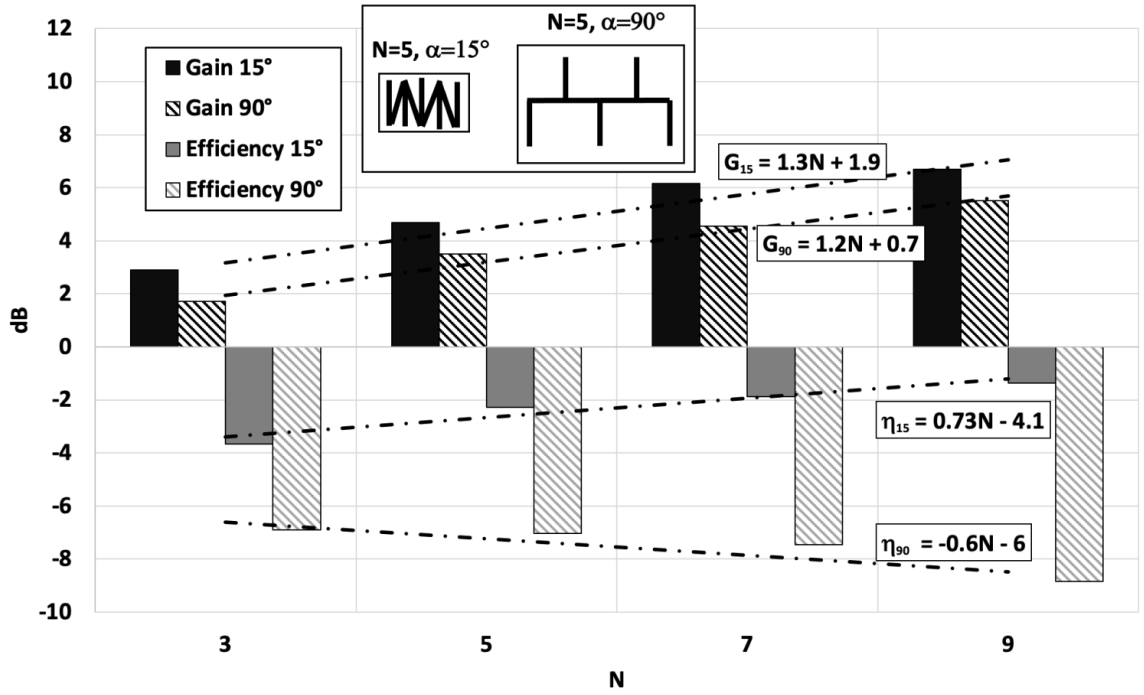

Fig. 4. Gain and radiation efficiency of the folded and the unfolded comb-line arrays ($\alpha = \{15^\circ, 90^\circ\}$) by varying the number of radiating elements. Dashed lines indicate the linear regressions. The area of the folded array is approximately 20% of the unfolded one, as in the inset.

Hence, two remarkable configurations can be defined: i) $\alpha = 45^\circ$ offers the maximum gain, ii) $\alpha = 15^\circ$ has maximum efficiency and minimal physical area. For these configurations, the effect of the substrate thickness h is numerically investigated in Fig.5. Regardless of the folding angle α, gain and efficiency improve with an increasing h before reaching a state of insensitivity to the substrate thickness, from about $h > 0.5$mm.

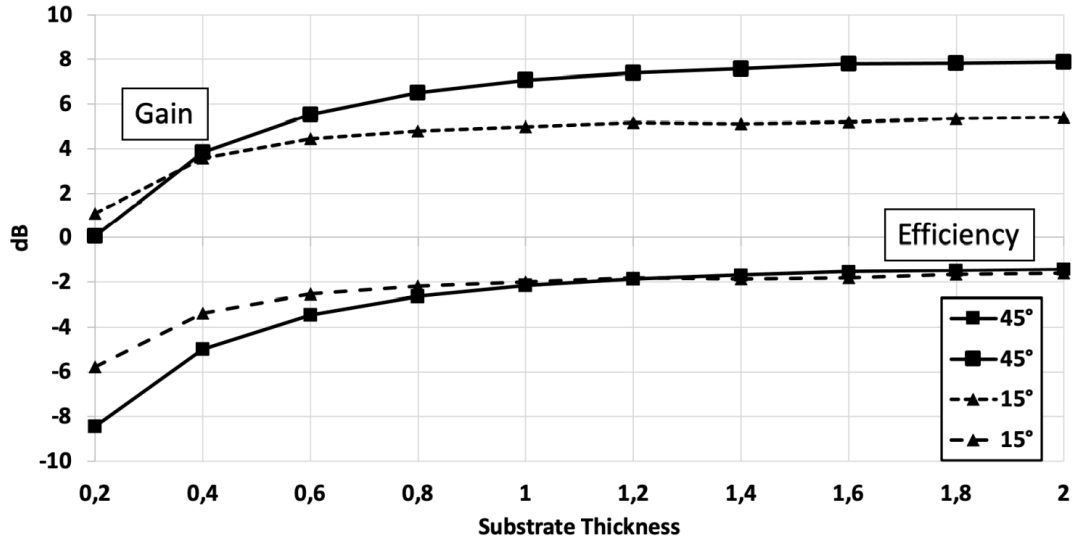

Fig. 5. Gain and radiation efficiency of the folded comb-line array (α = {15◦, 45◦}, N = 5) over increasing substrate thickness.

C. Input Impedance

Starting from $\{l, t\}$ = λwg/2, the length of the segments can be slightly changed such to make the antenna resonant and to obtain the proper pattern of current as in Fig.1. To tune the antenna to a particular input impedance, two additional parameters are considered; the length of the central vertical dipole l' and the position of the feeding point ΔF with respect to the centre of the dipole. Especially for small variations of the length, the former mainly impacts on the resonant frequency and hence on the imaginary part of the input impedance, while the latter acts on the real part (Fig.6).

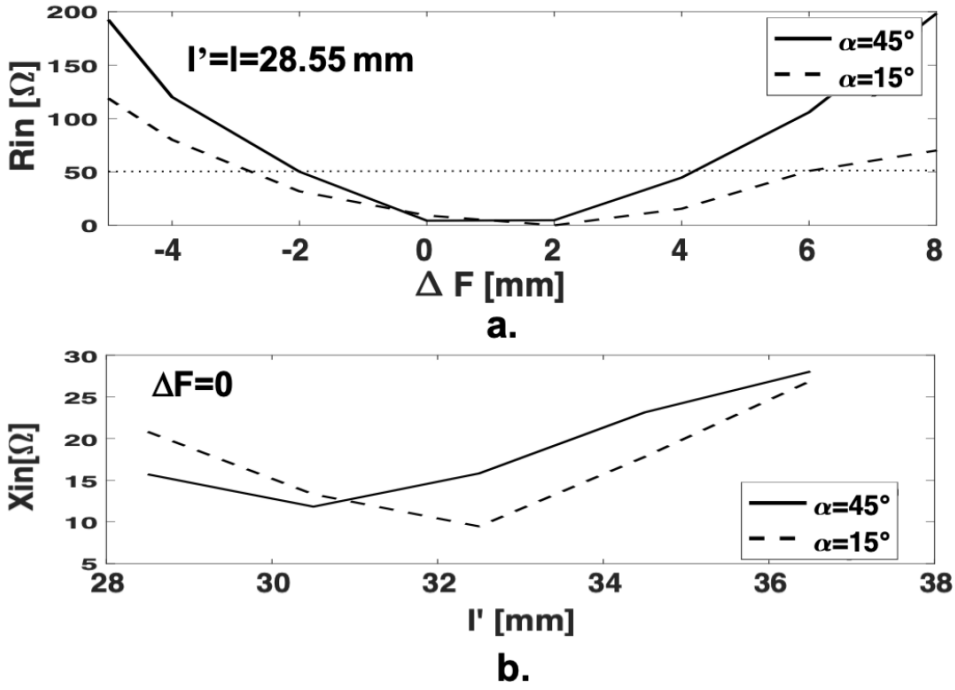

Fig. 6. Input impedance Zin versus the feeding position ΔF (a.) and the length of the central element l' (b). N = 5 array.

III. PROTOTYPE AND TEST

A prototype of the miniaturized N = 5 array with α = 15◦ has been fabricated and experimentally characterized. Since backscattering microchips are not yet available at 3.6 GHz, the antenna was matched to ZL = 50 Ω. For the sake of prototyping (especially in terms of sourcing materials during pandemic), the dielectric is a h = 0.762 mm Astra MT77 laminate from Isola Group, with ϵr = 3 and tanδ = 1.7·10−3. Although the selected substrate is semi-rigid, it was selected since it was easily procurable and can be easily wrought through a numerically controlled machine. However, as stated in the previous Sections, flexible and lightweight elastomeric substrates should be preferred [23], since they guarantee the conformability to the human body and increase the acceptance by the user.

Starting from λwg, parameters l and t have been slightly varied in simulation to obtain the proper pattern of current at the operating frequency, corresponding to five dipoles radiating in phase plus four slanted dipoles. Finally, impedance was tuned by moving the feeding point along the central dipole length. Simulated results are visible in Fig.7.

A prototype was fabricated with a numerical milling machine (inset in Fig. 8). An SMA connector was used to feed the antenna. The inner conductor was connected to the upper microstrip, while the outer was soldered on the ground plane.

S11 was measured by vector network analyser (HP 8517A) with the antenna attached onto a cubic body phantom (cooked pork with estimated parameters ϵr = 40 and sv = 2 S/m [7]). To reduce the impact of the cable, it was passed through the phantom and then connected to the VNA behind (see Fig.8 inset). The antenna required marginal manual tuning to 3.6 GHz by acting on the length of the fed dipole to compensate for uncertainties in realization and the phantom. Consequently, a good match was obtained (see Fig. 8), in agreement with the simulations. The bandwidth is BW−10dB ∼ 1.1% ≈ 40MHz for both simulation and measurements. Thanks to the decoupling ground plane and the path of the VNA cable through the phantom, measurements were robust and repeatable.

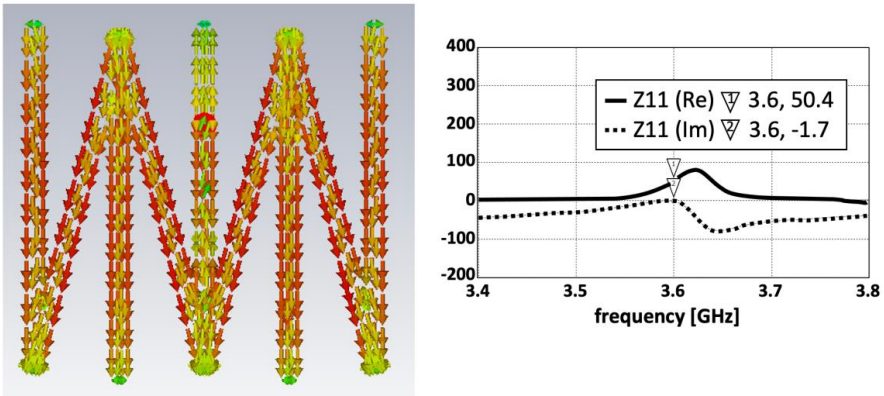

Fig. 7. Simulated pattern of current (a) and input impedance (b) of the N = 5, α = 15◦ folded comb-line. Standing waves on each segment are clearly visible.

Radiation performance of the array was estimated by applying the gain-comparison method [24]. A reference patch antenna with known gain (G0 = 2.2dB) [25] was measured on the same body phantom and in the same geometrical arrangement of the array under test. A Gmax ∼ 3.7dB with BW_{-3dB} (0◦,

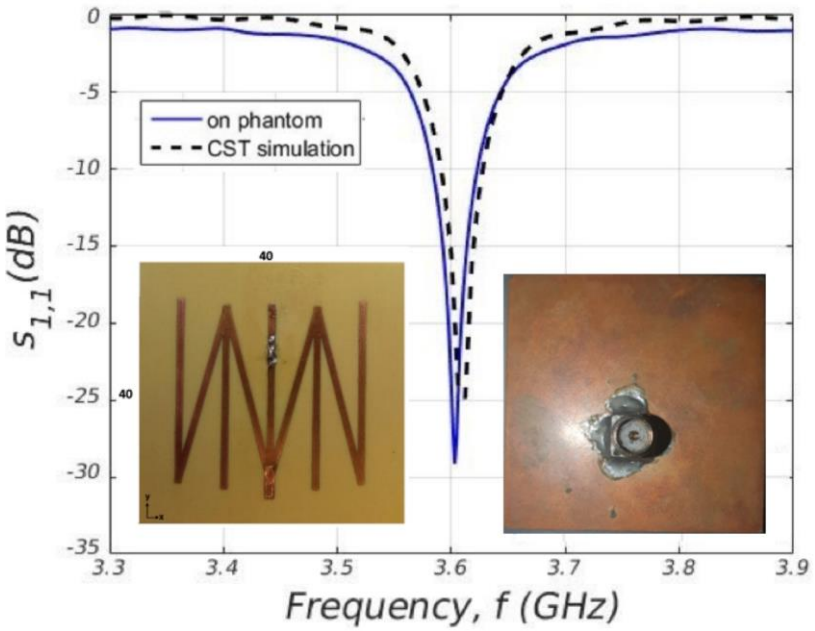

Fig. 8. Simulated and measured S11 on body phantom. Insets: Prototype of the folded comb-line etched on Astra MT77 laminate. Parameters $\{l, l', t, f, N, w, h, L, W\}$ = {28, 30, 28.25, 5.75, 5, 1, 0.762, 40, 40} mm, α = 15◦.

Radiation performance of the array was estimated by applying the gain-comparison method [24]. A reference patch antenna with known gain (G0 = 2.2dB) [25] was measured on the same body phantom and in the same geometrical arrangement of the array under test. A Gmax ∼ 3.7dB with $BW_{-3\text{dB}}$ (0◦, 90◦) = {67.5 ◦, 135◦} was retrieved and is fully in line with the simulations (|Gmax−sym − Gmax−meas| ≈ 0.9dB) on both vertical and horizontal planes (Fig. 9).

A. On-Body measurements

The prototype was also characterized in a real scenario. S11 and broadside gain were measured on a male volunteer when the device was placed in different body positions (Fig.10 top), namely at the armpit, knee, palm, back of the hand, and elbow. To reduce the impact of the cable, it was passed through gaps around the arm, leg, and fingers so that it was hidden by the body and then connected to the VNA behind.

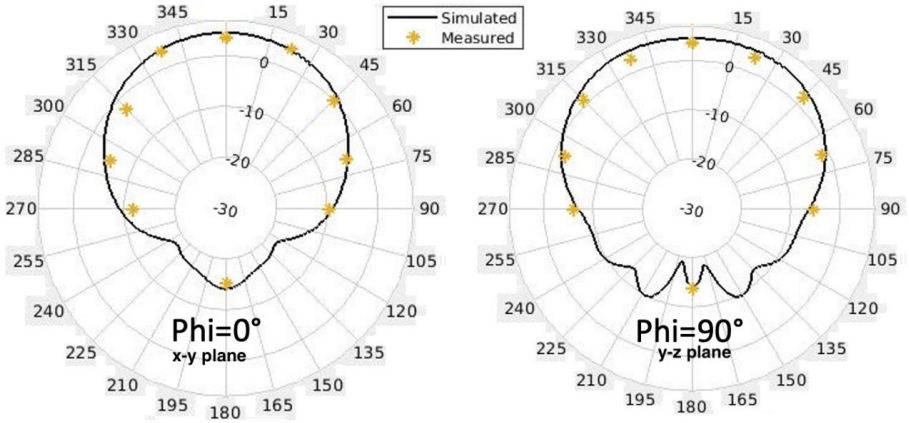

Fig. 9. Simulated and measured radiation pattern on the horizontal (Phi = 0 ◦) and vertical plane (Phi = 90◦).

The decoupling ground makes the antenna insensitive to the body, with S11 (see Fig.10 bottom) appearing stable and in good agreement with simulations, regardless of the position.

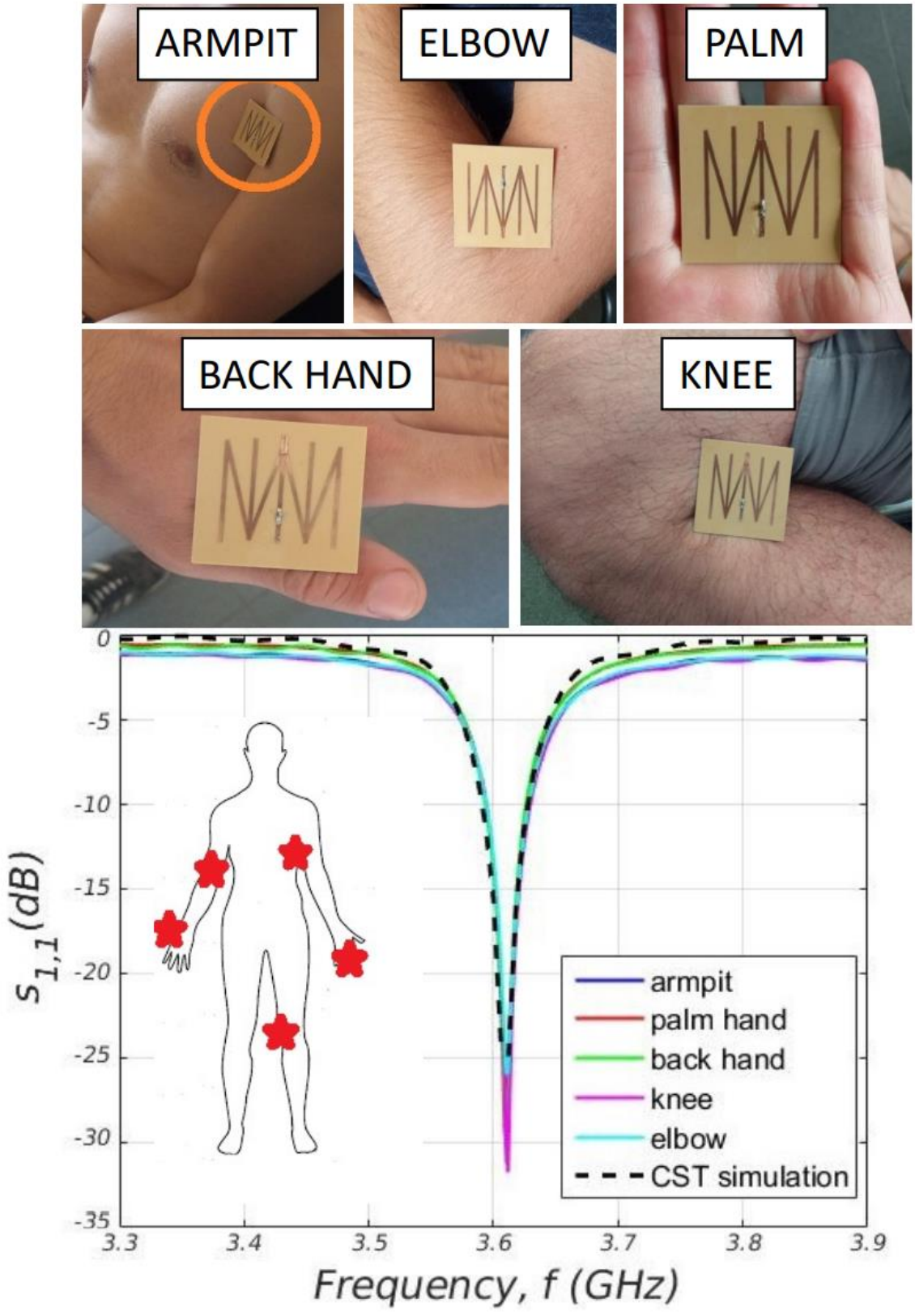

Fig. 10. Measured S11 of the antenna placed on different body regions of a male volunteer.

Similar consideration can be done for the gain (see Fig.11). Except for the armpit region (where the presence of a larger area of the body increases the array directivity) the maximum gain in the broadside direction ranges between 3 and 4 dB, in agreement with the measurements on the phantom.

Similar consideration can be done for the gain (see Fig.11). Except for the armpit region (where the presence of a larger area of the body increases the array directivity) the maximum gain in the broadside direction ranges between 3 and 4 dB, in agreement with the measurements on the phantom.

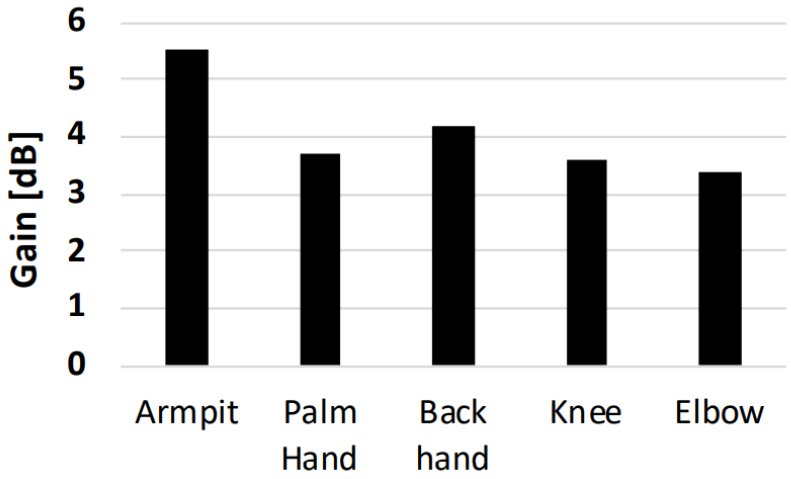

Fig. 11. Measured broadside gain of the antenna (peak values) placed on different body regions of a male volunteer.

B. Conformability

To evaluate the conformability of the array to curved body regions, the antenna was bent over a cylinder of diameter D = 8.5cm emulating arms or legs. S11 and the maximum gain were measured for the flat configuration and for the two bendings, over the E-plane and over the H-plane respectively. Since the prototype is semi-rigid, bending over the cylinder was forced through adhesive tape. Despite the different measurement conditions (the cylinder is an empty cardboard), S11 and broadside gain are in-line with the flat configurations (Fig.12). Bending produces minimal variations of the input impedance, however S11 < −12 dB at 3.6 GHz regardless of the configuration. The gain appears stable, showing bending had a negligible impact (< 0.5dB), confirming the conformability of the miniaturized device.

IV. CONCLUSIONS

A thin monolithic antenna array has been proposed for on-body applications at the 5G sub 6 GHz band as an evolution of the traditional comb-line array. The proposed layout offers better performance in terms of both efficiency and gain as well as a miniaturized footprint. The antenna is robust against positioning over the body. Furthermore, the smallest 4 cm×4 cm×0.1 cm configuration proved to be conformable to curved surfaces, with almost invariable input impedance and gain. The achieved size is compliant with typical epidermal plaster-like UHF tag antennas. Expected read distances are similar to what could be achieved by wearable UHF tags of comparable surface area, but with the additional benefits of the 5G frequencies. Such distances could be suitable for Personal Area Network (PAN) applications or to continuously track the vital signs of a user within a room, thus greatly extending on the current performances of UHF body-centric systems. Furthermore, since flexible elastomeric substrates capable to conform to the different body regions can be adopted, the layout is suitable to be worn on different body areas, such as shoulders, abdomen, arms and even on the head. Finally, to reduce the impact on the body and hence improve the wearability of the device, the ground can be trimmed around the comb-line profile or replaced by conductive fabrics.

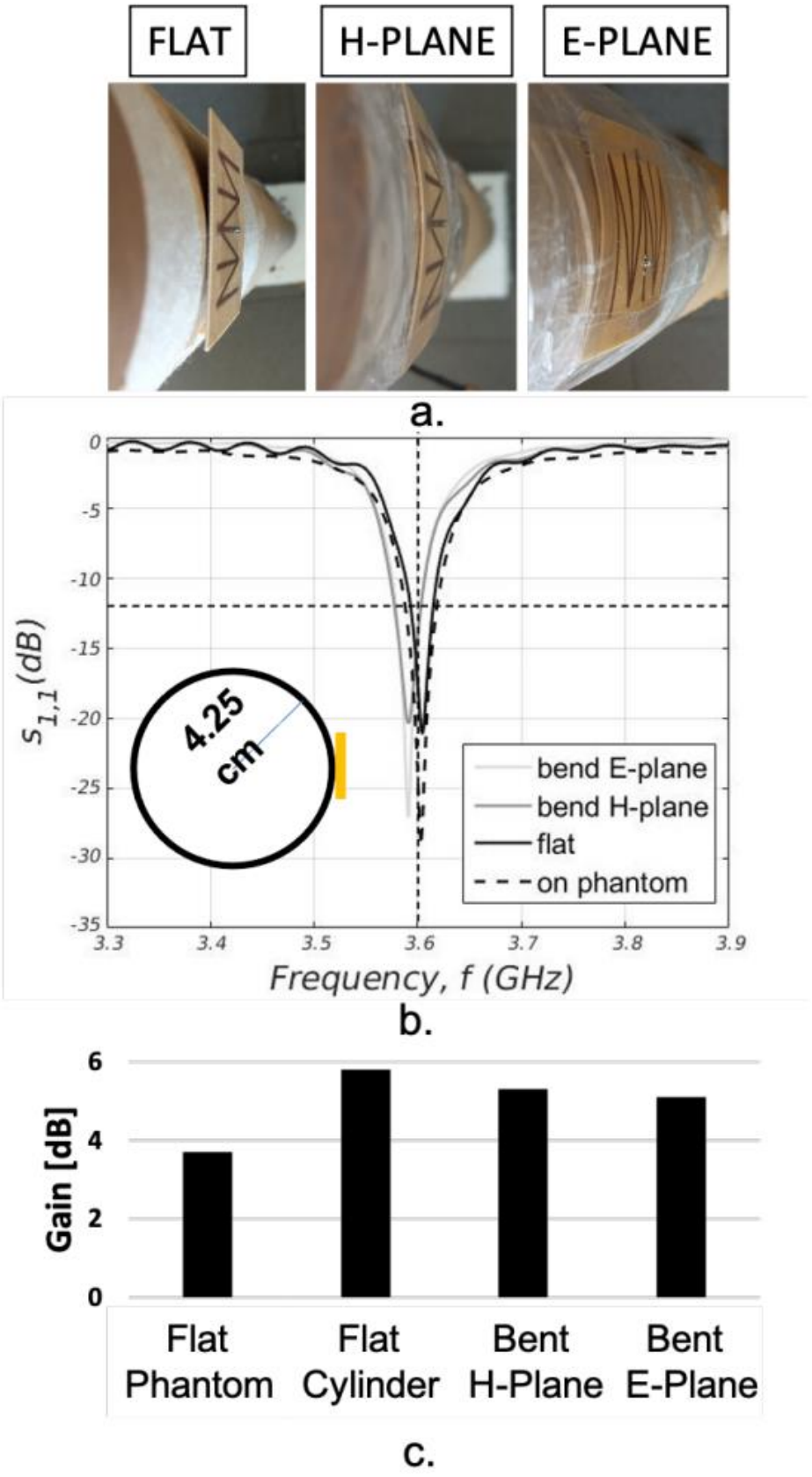

Fig. 12. Conformability analysis. The array was bent over a cylindric cardboard tube with a radius of 4.25 cm on the E and H planes (a). Measured S11 (b) and measured broadside gain (peak values) (c).

REFERENCES

[1] H. Habibzadeh, K. Dinesh, O. Rajabi Shishvan, A. Boggio-Dandry, G. Sharma, and T. Soyata, "A survey of healthcare internet of things (hiot): A clinical perspective," IEEE Internet of Things Journal, vol. 7, no. 1, pp. 53–71, 2020.

[2] J. C. Batchelor, R. J. Horne, P. S. Taylor, and M. I. Sobhy, "Rfid monitoring for assistive technologies beyond the clinic," in 12th European Conference on Antennas and Propagation (EuCAP 2018), April 2018, pp. 1–4.

[3] C. Yao, Y. Liu, X. Wei, G. Wang, and F. Gao, "Backscatter technologies and the future of internet of things: Challenges and opportunities," Intelligent and Converged Networks, vol. 1, no. 2, pp. 170–180, 2020.

[4] J. G. Andrews, S. Buzzi, W. Choi, S. V. Hanly, A. Lozano, A. C. K. Soong, and J. C. Zhang, "What will 5G be?" IEEE Journal on Selected Areas in Communications, vol. 32, no. 6, pp. 1065–1082, June 2014.

[5] N. F. M. Aun, P. J. Soh, A. A. Al-Hadi, M. F. Jamlos, G. A. E. Vandenbosch, and D. Schreurs, "Revolutionizing wearables for 5G: 5G technologies: Recent developments and future perspectives for wearable devices and antennas," IEEE Microwave Magazine, vol. 18, no. 3, pp. 108–124, May 2017.

[6] H. Ullah, N. Gopalakrishnan Nair, A. Moore, C. Nugent, P. Muschamp, and M. Cuevas, "5G communication: An overview of vehicle-toeverything, drones, and healthcare use-cases," IEEE Access, vol. 7, pp. 37 251–37 268, 2019.

[7] F. Amato, C. Occhiuzzi, and G. Marrocco, "Epidermal backscattering antennas in the 5g framework: Performance and perspectives," IEEE Journal of Radio Frequency Identification, pp. 1–1, 2020.

[8] F. Romoli Venturi, C. Occhiuzzi, and G. Marrocco, "Design and experimental characterization of on-skin loop antenna for next 5g backscattering-based communications," in Proceedings of the SpliTech2021, pp. –, year=2021.

[9] J. D. Hughes, C. Occhiuzzi, J. C. Batchelor, and G. Marrocco, "Twin grid-array as 3.6 ghz epidermal antenna for potential backscattering 5g communication," IEEE Antennas and Wireless Propagation Letters, 2020.

[10] L. Zhang, W. Zhang, and Y. P. Zhang, "Microstrip grid and comb array antennas," IEEE Transactions on Antennas and Propagation, vol. 59, no. 11, pp. 4077–4084, 2011.

[11] Y. Hayashi, K. Sakakibara, M. Nanjo, S. Sugawa, N. Kikuma, and H. Hirayama, "Millimeter-wave microstrip comb-line antenna using reflection-canceling slit structure," IEEE Transactions on Antennas and Propagation, vol. 59, no. 2, pp. 398–406, 2010.

[12] M. Sun, Y. P. Zhang, Y. Guo, K. Chua, and L. Wai, "Integration of grid array antenna in chip package for highly integrated 60-ghz radios," IEEE Antennas and Wireless Propagation Letters, vol. 8, pp. 1364–1366, 2009.

[13] B. Zhang and Y. P. Zhang, "Analysis and synthesis of millimeter-wave microstrip grid-array antennas," IEEE Antennas and Propagation Magazine, vol. 53, no. 6, pp. 42–55, 2011.

[14] D.-H. Shin, S.-J. Park, J.-W. Ahn, K.-W. Han, and S.-O. Park, "Design of shorted parasitic rhombic array antenna for 24 ghz rear and side detection system," IET Microwaves, Antennas & Propagation, vol. 9, no. 14, pp. 1581–1586, 2015.

[15] K. Hirose, K. Shinozaki, and H. Nakano, "A comb-line antenna modified for wideband circular polarization," IEEE Antennas and Wireless Propagation Letters, vol. 14, pp. 1113–1116, 2015.

[16] M. Mosalanejad, I. Ocket, C. Soens, and G. A. Vandenbosch, “Multilayer compact grid antenna array for 79 ghz automotive radar applications,” IEEE Antennas and Wireless Propagation Letters, vol. 17, no. 9, pp. 1677–1681, 2018.

[17] J. D. Hughes, C. Occhiuzzi, J. Batchelor, and G. Marrocco, “Folded comb-line array for healthcare 5g-rfid-based iot applications,” in 2021 IEEE International Conference on RFID (RFID). IEEE, 2021, pp. 1–5.

[18] H. Nakano, T. Kawano, and J. Yamauchi, “Meander-line grid-array antenna,” IEE Proceedings - Microwaves, Antennas and Propagation, vol. 145, no. 4, pp. 309–312, 1998.

[19] R. Conti, J. Toth, T. Dowling, and J. Weiss, “The wire grid microstrip antenna,” IEEE Transactions on Antennas and Propagation, vol. 29, no. 1, pp. 157–166, 1981.

[20] S. Orfanidis, Electromagnetic Waves and Antennas. New Jersey: Rutgers University, August 2010.

[21] M. Sun, Y. P. Zhang, Y. X. Guo, K. M. Chua, and L. L. Wai, “Integration of grid array antenna in chip package for highly integrated 60-ghz radios,” IEEE Antennas and Wireless Propagation Letters, vol. 8, pp. 1364–1366, 2009.

[22] N. Uzunoglu, N. Alexopoulos, and J. Fikioris, “Radiation properties of microstrip dipoles,” IEEE Transactions on Antennas and Propagation, vol. 27, no. 6, pp. 853–858, 1979.

[23] Laird, “Eccostock flexk:flexible dielectric elastomer,” https://www.laird.com/products/microwave-absorbers/low-lossdielectrics/eccostock-flexk,, 2021.

[24] C. A. Balanis, Antenna theory: analysis and design. John Wiley & Sons, Inc, 2016.

[25] C. O. P. T. F. Amato, A. Di Carlofelice and G. Marrocco, “S-band testbed for 5g epidermal rfids,” in URSI GASS 2020, Rome, Italy, 29 August - 5 September 2020), 2020, pp. 1–3.

[26] K. Finkenzeller, RFID Handbook: Fundamentals and Applications in Contactless Smart Cards and Identification, 2nd ed. New York, NY, USA: John Wiley and Sons, Inc., 2003.

[27] S. Manzari, S. Pettinari, and G. Marrocco, “Miniaturised wearable uhf-rfid tag with tuning capability,” Electronics Letters, vol. 48, no. 21, pp. 1325–1326, October 2012